JOURNAL OF PROPULSION AND POWER
Vol. 25, No. 6, November–December 2009

Forced Flame Response of Turbulent Liquid-Fueled Lean-Direct-Injection Combustion to Fuel Modulations

Tongxun Yi* and Domenic A. Santavicca†
Pennsylvania State University, State College, Pennsylvania 16802

DOI: 10.2514/1.42379

Reported are the forced flame responses of a turbulent, liquid-fueled, swirl-stabilized, lean-direct-injection combustor to fuel modulations. Fuel modulations are achieved using a motor-driven, high-frequency, rotary fuel valve specially designed for this experiment. This valve is capable of fuel modulations up to 1 kHz. The instantaneous fuel flow rate out of a fuel injector is accurately determined from pressure measurements at one or two locations upstream of the fuel nozzle. Linear flame responses are obtained with small-amplitude fuel modulations, typically below 2.0% of the mean fuel flow rate, about 60 Hz below the acoustic resonant frequencies. The invariance in the flame transfer functions to the fuel modulation amplitude suggests that the derived flame transfer functions are linear and that the induced heat release rate oscillations mainly respond to variations in the instantaneous fuel flow rate rather than in the droplet size and distribution. Flame transfer functions at different air flow rates, equivalence ratios, and preheat temperature are examined. With fuel modulations around the acoustic resonant frequencies, forcing-induced acoustic feedback on heat release responses cannot be ignored, and the measured flame transfer functions are no longer open-loop and linear. The nonlinearity in the forced flame responses is significantly affected by acoustic damping. Extinction and entrainment of self-excited combustion oscillations by fuel modulations at the approach of the acoustic resonant frequencies are observed. Self-excited combustion oscillations can be diminished by increasing the amount of fuel modulations. Applications of the flame transfer functions to modeling and control of combustion instability and lean blowout for both liquid-fueled and gas-fueled combustion are discussed.

Nomenclature

$\tilde{A}$	=	complex amplitude of the downstream-propagating acoustic wave, Pa
$\tilde{B}$	=	complex amplitude of the upstream-propagating acoustic wave, Pa
c	=	sound speed, m/s
$\bar{c}$	=	mean sound speed, m/s
D_a	=	Damköhler number
i	=	complex symbol
k	=	wave number, $\omega/\bar{c}$
M	=	mean flow Mach number, negligibly small in the present experiments, $\bar{u}/\bar{c}$
$\dot{m}'(t)$	=	perturbations in the instantaneous fuel flow rate out of a fuel injector, kg/s
$\bar{\dot{m}}_f$	=	mean fuel flow rate out of a fuel injector, kg/s
$\tilde{P}(x,t)$	=	complex dynamic pressure, Pa
$\tilde{P}_0(x,t)$	=	complex pressure immediately upstream of the fuel nozzle, Pa
$\tilde{P}_1(x,t)$	=	complex pressure at one location upstream of the fuel nozzle, Pa
$\tilde{P}_2(x,t)$	=	complex pressure at another location upstream of the fuel nozzle, Pa
$p_m(t)$	=	dynamic pressure measured at 0.29 m upstream of the fuel injector, Pa
$p_0(t)$	=	dynamic pressure immediately upstream of the fuel injector, Pa
$\tilde{R}$	=	specific acoustic impedance
Re()	=	real part of a complex quantity
S_L	=	laminar burning velocity, m/s
s	=	symbol of the Laplace transform
$\tilde{U}_0(t)$	=	complex acoustic velocity immediately upstream of a fuel nozzle, m/s
$\bar{u}$	=	mean velocity, m/s
$W_N(s)$	=	transfer function between pressure measurements and prediction immediately upstream of the fuel nozzle
x_m	=	pressure measurement location, 0.29 m upstream of the fuel nozzle, m
Z	=	symbol of the Z transform
α	=	thermal diffusivity, m^2/s
$\overline{\Delta P}$	=	mean pressure drop across the fuel nozzle, Pa
δ_L	=	laminar flame thickness, m
$\bar{\rho}$	=	mean density, kg/m^3
τ	=	residence time, s
τ_c	=	chemical reaction time, s
τ_V	=	evaporation time, s
ϕ	=	equivalence ratio

Received 25 November 2008; revision received 3 June 2009; accepted for publication 26 July 2009.

*Postdoctoral Fellow, Department of Mechanical and Nuclear Engineering; tzy1@psu.edu. Member AIAA.

†Professor, Department of Mechanical and Nuclear Engineering; das8@psu.edu. Member AIAA.

I. Introduction

COMBUSTION instability and lean blowout (LBO) are two major technical challenges for both gas-fueled and liquid-fueled dry-low-emission combustion [1]. Combustion instability refers to the self-excited, large-amplitude, limit-cycle thermoacoustic oscillations caused by the positive feedback between pressure and heat release. Strong pressure pulsations shorten engine life due to enhanced heat transfer, exacerbate NO_x emissions, generate noise pollutions, and cause instrumentation failures. LBO refers to partial or global flame quenching when the equivalence ratio is decreased below certain thresholds. As the equivalence ratio approaches the lean flammability limits, a combustor's resistance to external disturbances or small deviations from the equilibrium points is considerably weakened [2]. Thus, a small external disturbance in the inlet turbulence, fuel composition, fuel flow rate, and/or air flow rate may quench the flame. LBO necessitates expensive shutdown and restarting procedures for land-based gas turbines and represents a major safety hazard for aircraft engines.

The underlying mechanisms for combustion instability and LBO are fundamentally different, but both make engines unable to operate in an efficient, safe, and environment-friendly manner at lean conditions. Model-based control design is a standard approach for control engineers and theorists. Low-order models can be developed from either first principles or experimental data. The measured flame transfer functions (FTFs) (i.e., heat release responses to inlet air and/or fuel modulations) provide accurate descriptions of combustion dynamics around the working conditions in which they are derived. To examine system dynamics within a broad working range, multiple experiments can be performed.

The FTF is determined by both the intrinsic dynamics of a specific combustor and the manner in which dynamic fuel is introduced into and dispersed inside the reacting flowfield. To minimize the amount of fuel modulations required, it is desirable for the FTF to have a large gain. This can only be achieved by maximizing the conversion of the modulated fuel flow rate to the modulated heat release rate. In gas turbine combustors, the heat release zone lies along the swirling shear layer outside the recirculating vortex breakdown. Because of the flowfield inhomogeneities and the convective time delay, the spatially and temporally coherent fuel modulations exiting the fuel nozzle become spatially dispersed and temporally less coherent as they are transported downstream, which lowers the FTF gain. The situation becomes even worse for long flames. Droplet size also plays a role in the heat release responses. Yu and Wilson [3] have noticed that the critical fuel flux (i.e., the minimum fuel modulations required to attenuate combustion instability) depends on the droplet size. A smaller droplet size reduces the heating and evaporation time and enhances the control effectiveness. This observation is consistent with the proposition that the dynamic evaporation process may play an important role in liquid-fueled combustion instability [4]. Droplet size, spatial distribution, and numerical density can be measured using a phase Doppler particle analyzer, Malvern sizers, combined Mie scattering and planar laser-induced fluorescence, and other means. Laser diagnostics of reacting and nonreacting dynamic sprays will be reported later.

The present study is an investigation of forced flame responses under fuel modulations, and the intended application is combustion control design. Systematic investigations of heat release responses to fuel modulations are rather scarce in combustion literature. However, the coupling between heat release and acoustic oscillations has been extensively studied both experimentally and theoretically, for lean premixed combustion in particular. The purpose of air modulations is to obtain forced flame responses at conditions similar to self-excited combustion oscillations. By combining acoustic modeling with the measured heat release responses, the onset and limiting amplitude of combustion instability could be predicted. A summary of low-order models for flame/acoustics/turbulence interactions ranging from the seminal integral approach pioneered by Marble and Candel [5] in the 1970s to the recent progress is provided by You et al. [6]. The models proposed by You et al. [6] have incorporated the effects of turbulence and acoustic oscillations on flame propagations. Preetham and Lieuwen [7] have also considered the effects of background turbulent motions on flame propagations. They report that turbulence decreases the amplitude of the forced flame responses. For partially premixed gas-fueled combustion, equivalence-ratio perturbations caused by the differential acoustic impedance between the fuel and air lines also affect the heat release dynamics via variations in the reaction heat, the laminar flame speed, and the flame surface area [8]. These modeling works suggest that the heat release responses of lean premixed combustion to velocity perturbations are governed by three relevant parameters: namely, the flame Strouhal number, which is defined as the ratio of the convection time along the flame front to the velocity oscillation period, the flame length, and the flame angle [9–11]. Because of mathematical tractability, these low-order models seldom consider the effects of gas expansion across the flame front, the baroclinic vorticity generation, and the coupling between the entropical, vortical, and acoustical modes along the spatially developing swirling shear layer. However, Kim et al. [12,13] report that these three parameters can be used to correlate the forced flame responses in their experiments. It is worthwhile to realize that both the flame length and the flame angle are phenomenological variables and are ultimately determined by the combustor geometry, the inlet velocity profile, turbulent intensity, and laminar flame speed. Considerable attention has been paid to the nonlinearity in the forced heat release responses. The nonlinearity has been found to be associated with the shear-layer rollup, large-vortex shedding, flame liftoff, and unsteady flame holding [14,15]. It is well known that large-vortex shedding synchronized with pressure cycles is a dominant mechanism for combustion instability in bluff-body-stabilized and dump combustors [16]. In such combustors, because of the strong backflow, the velocity profile exhibits a deflection point across the separating shear layer; thus, the shear flow is particularly susceptible to the self-excited, absolutely unstable, large-scale vortex shedding [17]. Shear-layer vortices and vortex shedding are significantly enhanced when air modulations are applied around the preferred frequency ranges. Out of these preferred frequency ranges, even with large-amplitude air forcing, the heat release responses can still be linear [14]. The swirling shear layer is typically more stable to inlet velocity perturbations. This is because the swirling shear layer has much faster growth and decay rates than the nonswirling counterparts; thus, there are fewer opportunities for the initial disturbances to continuously grow into large vortices [18,19]. In the present swirl-stabilized combustor, no large-vortex shedding is observed, even when the pressure amplitude exceeds the pressure drop across the air swirler [20]. Several other researchers have also observed the invariance of flame structure in swirl-stabilized combustors during combustion oscillations [21,22]. Kim et al. [12] report the formation of large-vortex shedding under air modulations in a turbulent swirl-stabilized combustor. However, flame stabilization in the combustor is mainly achieved by gas recirculation behind a recessed centerbody instead of the aerodynamic processing vortex core.

This paper is organized as follows. First, the experimental setup is described, including the combustion rig, the optical setup, and the high-frequency rotary valve. Second, a method for determination of the instantaneous fuel flow rate out of a fuel nozzle is presented. This method is based on the acoustic wave theory and pressure measurements upstream of the fuel nozzle. Third, the FTFs at different air flow rates, equivalence ratios, and preheat temperature are reported. Fourth, the nonlinear forced flame responses around the acoustic resonant frequencies are presented. Finally, we discuss potential applications of the FTFs to combustion instability control and LBO extension.

II. Experiment Setup

Figure 1 shows the combustion rig, the optical setup, and the rotary fuel valve. Preheated air enters a quartz combustion chamber, 0.10 m in diameter and 0.30 m in length, through a 30 deg radial-entry swirler. The exit diameter of the swirler is 3.56 cm. The radial swirler has eight tangential-entry ports. Flow separation and reunion across the swirler generate significant amount of streamwise vortices, which effectively enhances droplet/vapor/air entrainment and mixing. Pressure drop across the air swirler varies with the air flow rate and the preheat temperature, but it is within 5% for all results reported here. One-decene or jet-A is injected into the swirling air flow 0.02 m upstream of the dump plane using a single-point macrolaminated fuel nozzle (2.5 gal/h) from Parker-Hannifin Corporation. With a pressure drop of 689 kPa across the fuel nozzle, the droplet Saunter mean diameter is less than 10 μm.[‡] The small droplet size and fast fuel/air mixing result in the flame spectra are very similar to lean premixed combustion. The air flow rate is measured using a vortex flowmeter from Omega, with a measurement uncertainty of 54 slpm. A photomultiplier tube (PMT) (H7732-10 from Hamamatsu Photonics) featured with an interference bandpass filter ($\sim$430 or $\sim$307 nm with full width at half-maximum of 10 nm) is used for global chemiluminescence measurements. Note that chemiluminescence should not generally be simply assumed to be proportional to the instantaneous heat release rate [23]. However, the instantaneous chemiluminescence intensity is a function of the instantaneous air consumption

[‡]Private communication with engineers from Parker-Hannifin Corporation, April 2008.

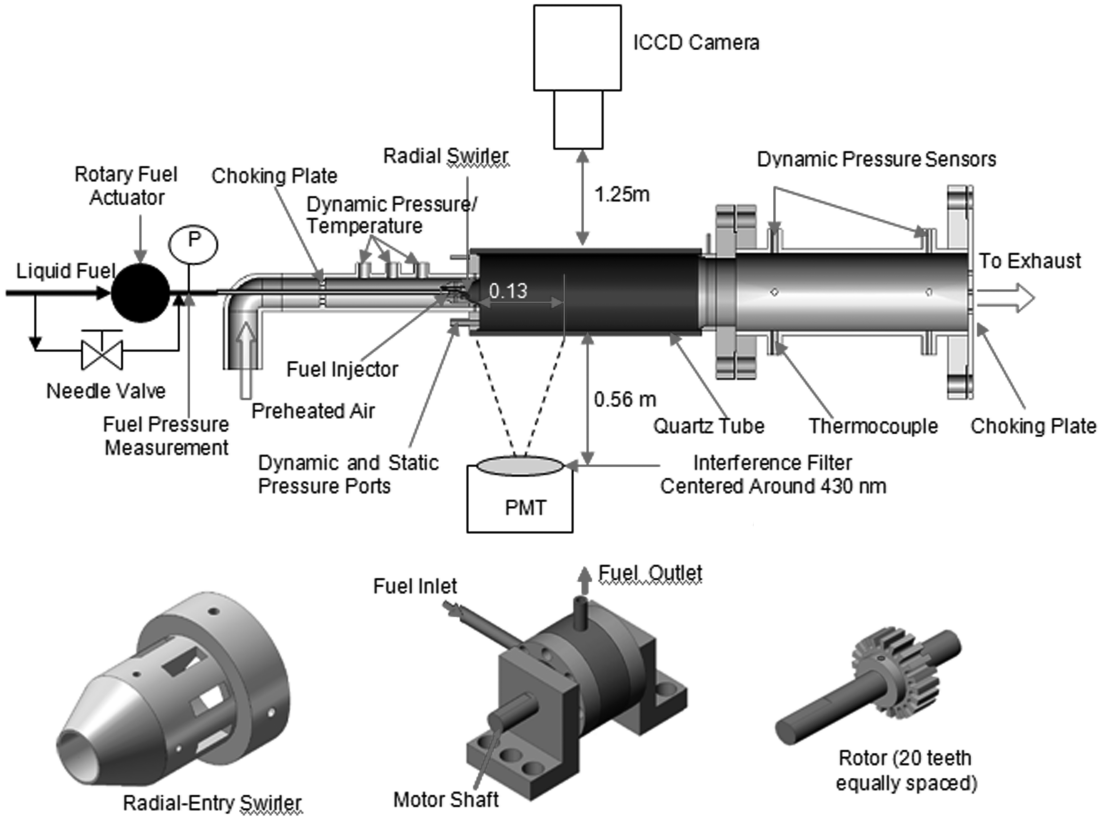

Fig. 1 Combustion rig, optical setup, and rotary fuel actuator.

rate, equivalence ratio, flame temperature, and acoustic oscillations; thus, it can serve as a useful indicator for the forced flame responses. The PMT is placed 0.06 m downstream of the dump plane and 0.56 m away from and perpendicular to the quartz chamber. The PMT viewing area is within 0.13 m downstream of the dump plane. Spectral measurements using an Oriel MS125^{TM} spectrograph (Fig. 2) show that the emission spectra within the UV visible range are very similar to those of lean premixed combustion. Also shown in Fig. 2 are the intensified charge-coupled-device images of OH* chemiluminescence at $\phi = 0.33$ and the preheat temperature of 423 K. The axial center of heat release lies at 2.5 cm downstream of the dump plane. Stable combustion is achieved by inserting three baffle plates downstream of the quartz combustion chamber. No self-excited combustion oscillations have been observed when the baffle plates are used.

Fuel modulations are achieved using a motor-driven rotary fuel valve specially designed for this experiment. The fuel modulation frequency is determined by the number of rotor teeth and the motor rotating speed. Liquid fuel is stored in a 19 liter stainless steel tank and pressurized with N_2 at 1378 kPa. The mean fuel flow rate is measured using a linear flow meter with an uncertainty of 5%. The mean fuel flow rate is controlled using a needle valve. The rotary valve is located 0.46 m upstream of the fuel nozzle. A 0.8 l accumulator is located 0.2 m upstream of the rotary valve. A Sensotec pressure transducer (sensitivity 172 kPa/V and uncertainty of 0.25%) capable of working up to 2 kHz is installed 0.29 m upstream of the fuel nozzle. A bypass flow passage is installed parallel to the rotary fuel valve, and the fuel modulation amplitude is controlled by varying the fuel split between the rotary fuel valve and the bypass passage. Figure 3 shows the fuel modulation ratio, which is defined as the ratio of the fuel pressure RMS to the mean fuel pressure. The fuel modulation ratio is greater than 30% below 750 Hz and greater than 15% up to 1 kHz.

III. Determination of the Instantaneous Fuel Flow Rate

The instantaneous fuel flow rate out of a fuel injector is an important parameter for combustion analysis and control. Unsteady fuel

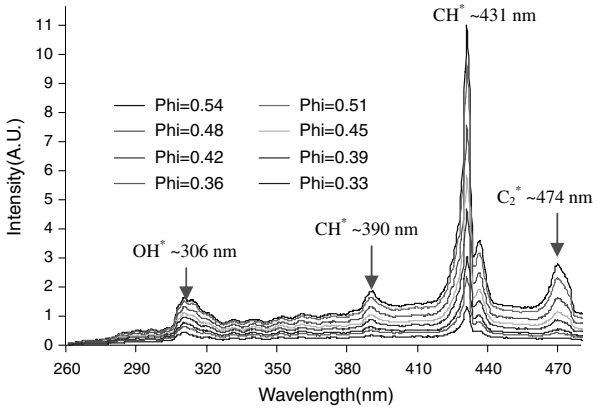

a)

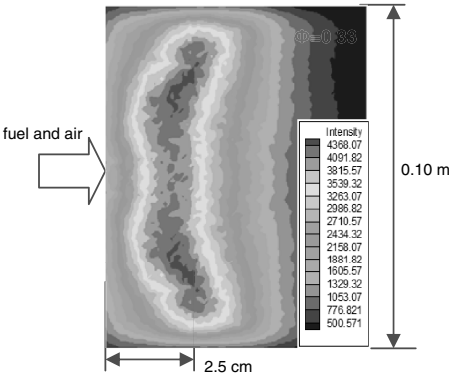

b)

Fig. 2 Flame spectra and ICCD imaging of OH* chemilumienscence for jet-A-fueled LDI combustion: a) flame spectra and b) ICCD imaging. Air flow rate is 44.5 g/s and preheat temperature is 423 K.

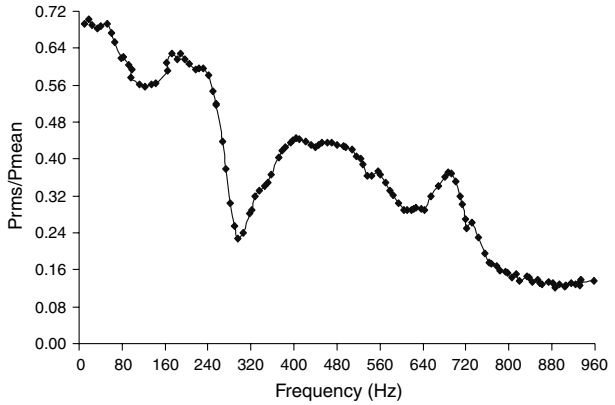

Fig. 3 Fuel modulation ratio with zero bypass flow. The mean fuel pressure upstream of the fuel nozzle is 152 kPa. A Parker-Hannifin fuel nozzle (5.0 gal/h) is used here.

flow rates into a combustor can be caused by both self-excited pressure pulsations and fuel modulations. The instantaneous fuel flow rate across the fuel injector is related to the instantaneous pressure drop across the fuel nozzle. However, pressure measurements immediately upstream of the fuel injector are extremely challenging in a production engine, because of the limited space and the harsh environment. Pressure measurements upstream of the fuel nozzle can differ considerably in both amplitude and phases from those immediately upstream of the fuel nozzle. A literature survey shows that accurate determination of the instantaneous fuel flow rate has not received much attention in the combustion community. In this paper, we present a method for accurate determination of the instantaneous fuel flow rate, which is based on the acoustic wave theory and pressure measurements at one or two locations upstream of the fuel nozzle. This method is an extension of a method for determination of fuel modulations out of a gaseous fuel nozzle [24]. For both methods, small-amplitude fuel modulations are assumed. In the case of large-amplitude fuel modulations (in particular, at high frequency), the 1-D nonlinear wave equations accounting for the nonlinear acoustics and viscous shear stress should be used. Solutions to nonlinear wave equations are less straightforward than those to linear waves. A simple method for validating the assumption of linear acoustics is to install a pressure transducer at another location in the fuel line and to compare pressure measurements with linear predictions.

To improve atomization, the pressure drop across a liquid-fueled, pressure-swirl, lean-direct-injection (LDI) nozzle is typically much higher than that across a gaseous fuel injector. Thus, the dynamic fuel pressure associated with flow acceleration along the streamline can be neglected, and a liquid-fueled, pressure-swirl, LDI nozzle can be modeled as a purely resistive element. For small-amplitude quasi-steady fuel modulations, the pressure wave within the fuel tubing is described by the following 1-D linear equation:

$$\tilde{P}(x,t) = \hat{P}(x)e^{i\omega t} = \tilde{A}e^{i(\omega t - \frac{kx}{1+M})} + \tilde{B}e^{i(\omega t + \frac{kx}{1-M})}$$

$$\tilde{U}(x,t) = \hat{U}(x)e^{i\omega t} = \frac{1}{\bar{\rho}\,\bar{c}}[\tilde{A}e^{i(\omega t - \frac{kx}{1+M})} - \tilde{B}e^{i(\omega t + \frac{kx}{1-M})}] \tag{1}$$

The complex amplitude of downstream- and upstream-propagating waves can be determined from pressure measurements at two locations upstream of the fuel nozzle:

$$\tilde{A} = \frac{\hat{P}_2 e^{ik(\frac{x_2}{1+M}+\frac{2x_1}{1-M^2})} - \hat{P}_1 e^{ik(\frac{x_1}{1+M}+\frac{2x_2}{1-M^2})}}{e^{ik\frac{2x_1}{1-M^2}} - e^{ik\frac{2x_2}{1-M^2}}} \quad \tilde{B} = \frac{\hat{P}_1 e^{ik\frac{x_1}{1+M}} - \hat{P}_2 e^{ik\frac{x_2}{1+M}}}{e^{ik\frac{2x_1}{1-M^2}} - e^{ik\frac{2x_2}{1-M^2}}} \tag{2}$$

where $\hat{P}_1$ and $\hat{P}_2$ are the complex pressure amplitude at upstream locations x_1 and x_2, respectively. The complex pressure amplitude is computed using fast Fourier transform (FFT). The specific acoustic impedance along the fuel tubing is determined as

$$\tilde{R}(x) = \bar{\rho}\,\bar{c}\frac{\tilde{A}e^{i(-\frac{kx}{1+M})} + \tilde{B}e^{i(\frac{kx}{1-M})}}{\tilde{A}e^{i(-\frac{kx}{1+M})} - \tilde{B}e^{i(\frac{kx}{1-M})}} \tag{3}$$

Pressure oscillations immediately upstream of the fuel nozzle are determined as (the origin is at the nozzle entrance)

$$\tilde{P}(0,t) = \hat{P}(0)e^{i\omega t} = (\tilde{A} + \tilde{B})e^{i\omega t} \tag{4}$$

Perturbations in the instantaneous fuel flow rate can be determined as

$$\frac{\dot{m}'_f}{\bar{\dot{m}}_f} = \frac{p_0(t)}{2\overline{\Delta P}} = \frac{Re(\tilde{P}(0,t))}{2\overline{\Delta P}} \tag{5}$$

The specific acoustic impedance $\tilde{R}(0)$ can also be determined from the linearized quasi-steady Bernoulli equation across the fuel nozzle:

$$\tilde{R}(0) = \bar{\rho}\,\bar{c}\frac{\tilde{A}+\tilde{B}}{\tilde{A}-\tilde{B}} = \frac{2\overline{\Delta P}}{\bar{u}} \Rightarrow \frac{\tilde{A}}{\tilde{B}} = \frac{2\overline{\Delta P} + \bar{\rho}\,\bar{c}\,\bar{u}}{2\overline{\Delta P} - \bar{\rho}\,\bar{c}\,\bar{u}} \tag{6}$$

In our tests, $2\overline{\Delta P}$ and $\bar{\rho}\,\bar{c}\,\bar{u}$ are of the same order. Figure 4 compares the predicted and measured dynamics pressure 0.04 m upstream of the fuel nozzle. In this experiment, three pressure transducers are installed at 1.04, 0.57, and 0.04 m upstream of the fuel nozzle, respectively. Resonance occurs around 250 Hz, and around this resonant frequency, the fuel modulation ratio is more than 30%. Differences between pressure measurements and prediction are within 6% in amplitude and 6 deg in phases. The errors are mainly associated with the uncertainties in pressure measurements and sound speed. By measuring the same pressure field using these three pressure transducers, we find that the differences in amplitude can be up to 3%, whereas the differences in phases can be up to 4 deg. Differences in frequency responses of the three pressure transducers have been considered for data analysis. The sound speed for 1-decene is not readily available from open literature, but it is believed to be similar

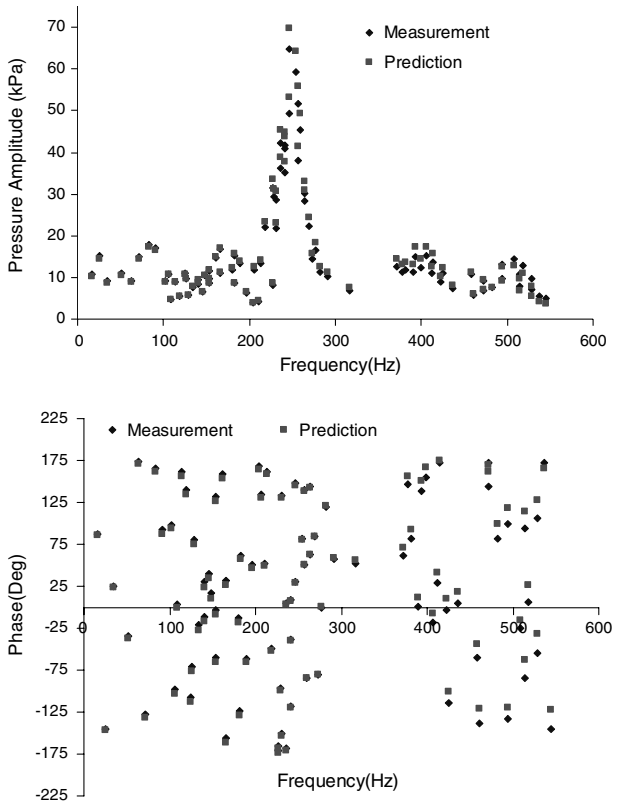

Fig. 4 Pressure measurements vs prediction at 0.04 m upstream of the fuel nozzle. The mean fuel pressure is 138 kPa. The sound speed of 1-decene is taken as 1100 m/s. The mean velocity inside the fuel tubing is 00.45 m/s. A Parker-Hannifin fuel nozzle (5.0 gal/h) is used here. The fuel setup for this experiment is different from that in Fig. 3.

to that of jet-A. The database of sound speed for jet-A is usually limited to pressure above 1000 kPa [25]. The sound propagating speed along the fuel tubing is a function of pressure, temperature, fuel species, wall elasticity, and bubbles. The sound speed increases with fuel pressure and wall elasticity and decreases substantially with temperature and bubbles. It is usually above 1000 m/s at room temperature [25]. Sound speed of 1100 m/s is found to give the best match between measurements and prediction. It is found that even without accounting for the nonlinear acoustics and viscous shear stress, the developed method can well predict large-amplitude pressure oscillations up to 30% below 300 Hz.

Equation (5) shows that for pressure-swirl nozzles, the instantaneous fuel flow rate $\dot{m}'_f(t)$ can be determined from the predicted fuel pressure immediately upstream of the fuel nozzle, $p_0(t)$. According to Eq. (1), $p_0(t)$ can be determined from $p_m(t)$ using the following relationship:

$$W_N(s=i\omega)=\frac{P_m(s)}{P_0(s)}=\frac{\tilde{A}e^{-s\frac{x_m}{\bar{c}(1+M)}m}+\tilde{B}e^{s\frac{x_m}{\bar{c}(1-M)}}}{\tilde{A}+\tilde{B}}$$
$$=\frac{\tilde{A}/\tilde{B}e^{-s\frac{x_m}{\bar{c}(1+M)}}+e^{s\frac{x_m}{\bar{c}(1-M)}}}{\tilde{A}/\tilde{B}+1}(x_m=-0.29\text{ m}) \tag{7}$$

where $P_m(s)$ and $P_0(s)$ refer to the Laplace transform of $p_m(t)$ and $p_0(t)$, respectively. Equation (7) shows that the gain of $W_N(s)$ decreases with frequency, whereas the phase increases. Here, we derive the fuel transfer function for the relationship between $\dot{m}'_f(t)$ and $p_m(t)$:

$$W_F(s=i\omega)=\frac{M_f(s)}{P_m(s)}=\frac{M_f(s)}{P_o(s)}\frac{P_0(s)}{P_m(s)}=\frac{\bar{\dot{m}}_f}{2\overline{\Delta P}}\frac{1}{W_N(s)} \tag{8}$$

IV. Linear Flame Responses

Linear flame responses are obtained by applying small-amplitude fuel modulations, typically below 2% of the mean fuel flow rate, about 60 Hz below the acoustic resonant frequencies. During fuel modulations, the mean fuel flow rate is maintained constant by adjusting the opening of a needle valve, and the forcing frequency is varied from 10 to 1 kHz, with a stepwise increment of about 10 Hz. During these measurements, the variations in the mean fuel pressure and CH* chemiluminescence are within 1.5%. The sampling frequency is 5 kHz, and the data length is 8 s. The data are decomposed into eight segments, and FFT analysis is performed for each second. Without explicit denotation, FTFs are the average of the results for the eight data segments.

The FTFs relating chemiluminescence to fuel modulations can be defined in multiple forms, such as $\mathrm{CH}^*(s)/P_0(s)$, $\mathrm{CH}^*(s)/M_f(s)$, and $\mathrm{CH}^*(s)/P_m(s)$. $\mathrm{CH}^*(s)$ denotes the Laplace transform of the overall CH* chemiluminescence intensity. Without explicit denotation, the FTFs are defined as

$$W(s=i\omega)=\frac{\mathrm{CH}^*(s)}{P_m(s)} \tag{9}$$

The convenience of this definition is that both CH* chemiluminescence and the fuel pressure are directly measured. Note that different forms of the flame transfer functions are convertible. For example,

$$\frac{\mathrm{CH}^*(s)}{P_0(s)}=\frac{\mathrm{CH}^*(s)}{P_m(s)}\frac{P_m(s)}{P_0(s)}=W(s)W_N(s)$$

and

$$\frac{\mathrm{CH}^*(s)}{M_f(s)}=\frac{\mathrm{CH}^*(s)}{P_m(s)}\frac{P_m(s)}{M_f(s)}=\frac{W(s)}{W_F(s)}$$

To be consistent with the definitions of FTFs in combustion literature [12,13], we also express the data in the following normalized FTFs:

$$\bar{W}(s=i\omega)=\frac{\bar{P}_m}{\overline{\mathrm{CH}^*}}\frac{\mathrm{CH}^*(s)}{P_m(s)} \tag{10}$$

In combustion literature, the FTFs for air modulations are usually defined as [10,12,13]

$$\frac{\bar{V}}{\overline{\mathrm{CH}^*}}\frac{\mathrm{CH}^*(s)}{V(s)}$$

where $\bar{V}$ and $\overline{\mathrm{CH}^*}$ refer to the mean velocity in the inlet pipe and the mean CH* chemiluminescence, respectively. Although the normalized FTFs defined by Eq. (9) may be elegant in presenting the data, it is not very convenient for control design. This is because the normalized FTFs require simultaneous measurements of the mean chemiluminescence and the mean fuel pressure.

Figure 5 shows the amplitude and phases of the measured FTFs up to 1 kHz. The FTF amplitude consistently increases with frequency up to 600 Hz, peaks around 750 Hz, and then drops. The irregularities in both the gain and phases of the FTFs between 600 and 660 Hz are caused by forcing-induced acoustic feedback. The blocking ratio at the inlet and the exit of the combustion chamber is 88 and 95%, respectively. Thus, the combustion chamber can be considered as acoustically closed at both ends. The resonant frequency of the one-wave mode is around 630 Hz. Although three baffle plates are inserted downstream of the combustion chamber, relatively large acoustic oscillations still occur with fuel modulations around 630 Hz. This in fact implies that the measured FTFs between 600 and 660 Hz are no longer open loop and linear. The FTF gain peaks around 720 Hz, which differs from the acoustic resonant frequencies. The distribution of the FTF gain with frequency is similar to a slightly damped higher-order (of at least second-order) system. This section focuses on the linear open-loop flame transfer functions below 600 Hz. Within this frequency range, forcing-induced acoustic oscillations are small. Note that the FTFs shown in Fig. 5 are defined

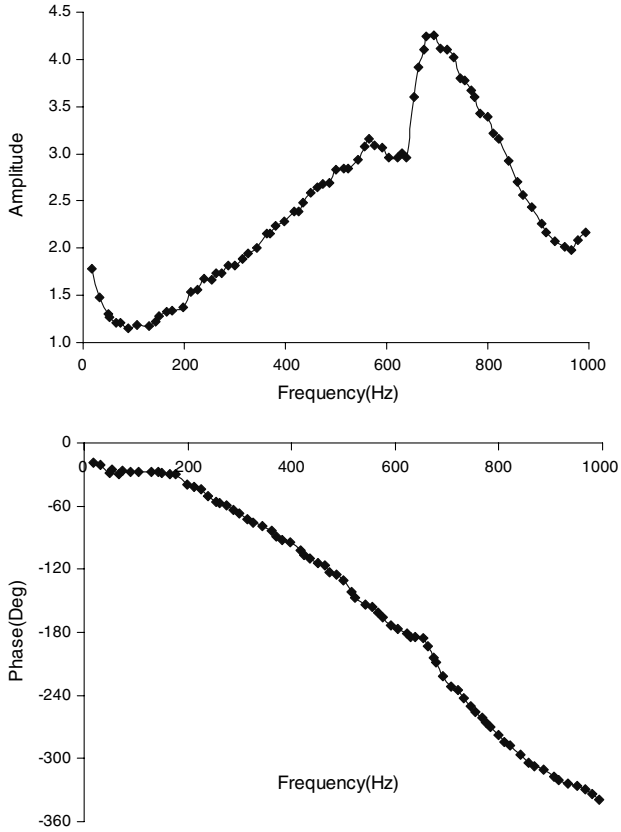

Fig. 5 Measured FTFs up to 1 kHz. The mean fuel pressure is 453 kPa, the air flow rate is 66.7 g/s, the equivalence ratio is 0.34, and the preheat temperature is 473 K. The fuel modulation ratio is typically below 2.0%. The combustor is fueled with 1-decene.

as $CH^*(s)/P_0(s)$. In this experiment, $\tilde{A}/\tilde{B}$ is determined from Eq. (6) as 1.80. According to Eq. (7), the gain of W_N consistently decreases with frequency up to 0.65 at 600 Hz, whereas the phase lag consistently increases with frequency up to 20.5 deg at 600 Hz.

A. Signal-to-Noise Ratio

The measured fuel pressure and CH^* chemiluminescence are inevitably contaminated by electrical noises, external disturbances, and quantization errors. CH^* chemiluminescence is intrinsically of a broadband or stochastic nature because of the large number of spatial and temporal scales in flame/turbulence interactions. For reliable FTFs to be developed, forcing-induced chemiluminescence must be stronger than the background noise [i.e., the signal-to-noise ratio (SNR) must be sufficiently high]. In our experiments, a SNR above 20 dB can be achieved with a fuel modulation ratio larger than 0.5%. Figure 6 shows the time traces of fuel pressure and chemiluminescence and their spectra with fuel modulations at 591 Hz. The fuel modulation ratio is 1.34%. Both the fuel pressure and chemiluminescence are filtered using a fourth-order Butterworth bandpass filter with bandwidth of 550–650 Hz. The SNR is higher than 32 dB for both fuel pressure and chemiluminescence, implying that the forced flame responses are suitable for FTF development.

B. Repeatability and Nonlinearity

The measured FTF is repeatable not only within the same sequence of experiments (see Fig. 7) but also among experiments conducted at different days (see Fig. 8). Even in the presence of self-excited, large-amplitude combustion oscillations (up to 12 kPa in amplitude) around 640 Hz, the FTF below 600 Hz is almost the same as that shown in Figs. 7 and 8. Strong repeatability in the FTF implies that meaningful and reliable FTFs have been obtained. One can see that below 600 Hz, the gain of the FTF for jet-A is almost the same as that for 1-decene, whereas above 320 Hz, the phase differences slightly increase with frequency up to 15 deg at 600 Hz. The differences in FFTs between jet-A and 1-decene are associated with the discrepancies in the evaporation rate and chemical kinetics. Jet-A has higher boiling points and is less volatile than 1-decene; thus, it takes a longer time for jet-A to evaporate. Also jet-A has more long-chain hydrocarbons than 1-decene; thus, the chemical reaction rate is lower.

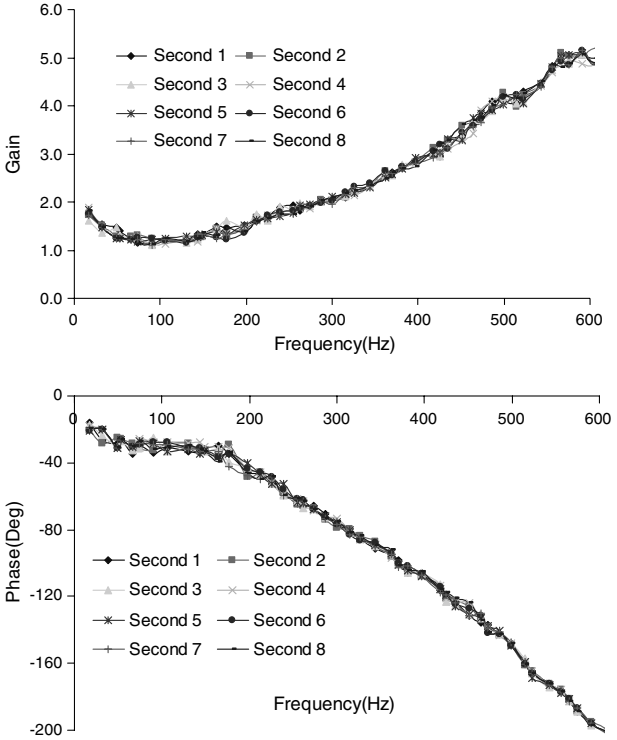

Fig. 7 FTFs within the same sequence of experiments. The mean fuel pressure is 453 kPa, the air flow rate is 66.7 g/s, the equivalence ratio is 0.34, and the preheat temperature is 473 K. The fuel modulation ratio is typically below 2.0%. The combustor is fueled with 1-decene.

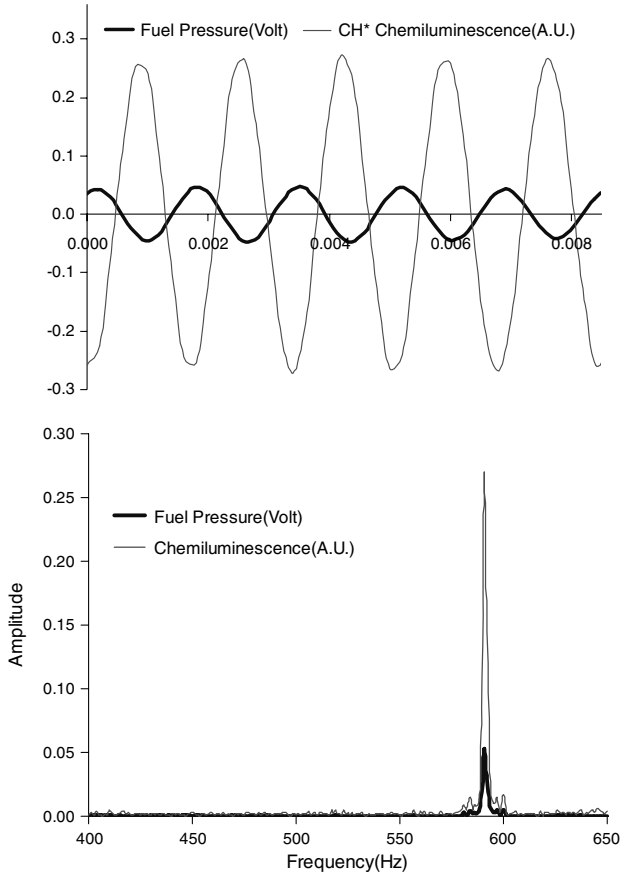

Fig. 6 Time traces of fuel pressure, chemiluminescence, and their spectra. The mean fuel pressure is 453 kPa, the air flow rate is 66.7 g/s, the equivalence ratio is 0.34, and the preheat temperature is 473 K.

Nonlinearity in the forced flame responses is checked by examining the variations in the FTFs with the fuel modulation amplitude. It is believed that the saturation thresholds above which nonlinear starts to appear depend on the forcing frequency and working conditions, such as the equivalence ratio, the preheat temperature, and the air flow rates. Figure 8b shows the fuel modulation ratios for the FTFs shown in Fig. 8a. Linearity in the forced flame responses is well kept, even in the presence of large fuel modulations more than 15% below 200 Hz.

C. Data-Driven Low-Order Models

The gain and phases of the measured FTFs shown in Fig. 8 can be accurately modeled by a low-order rational transfer function. Such low-order models are very convenient for combustion analysis and control. However, before the low-order models are developed, it is worthwhile to further explore system dynamics from the measured FTFs.

A plateau appears in phases of the FTFs between 50 and 200 Hz. This is mainly because within this frequency range, the forcing period is much longer than the time scales of fuel convection, evaporation, and chemical kinetics. ICCD imaging of OH^* chemiluminescence shows that at $\phi = 0.34$ and the preheat temperature of 473 K, the flame is rather short and major heat release is completed within 3.5 cm downstream of the dump plane. If the average axial velocity along the swirling shear layer is assumed as 40% of the swirler exit velocity (i.e., 36 m/s), then the convective time delay can be determined as 1 ms. If we assume a representative droplet size of 18 μm and the representative temperature of 900 K, and if we neglect velocity slip, droplet interactions, initial transients, and radiative heat

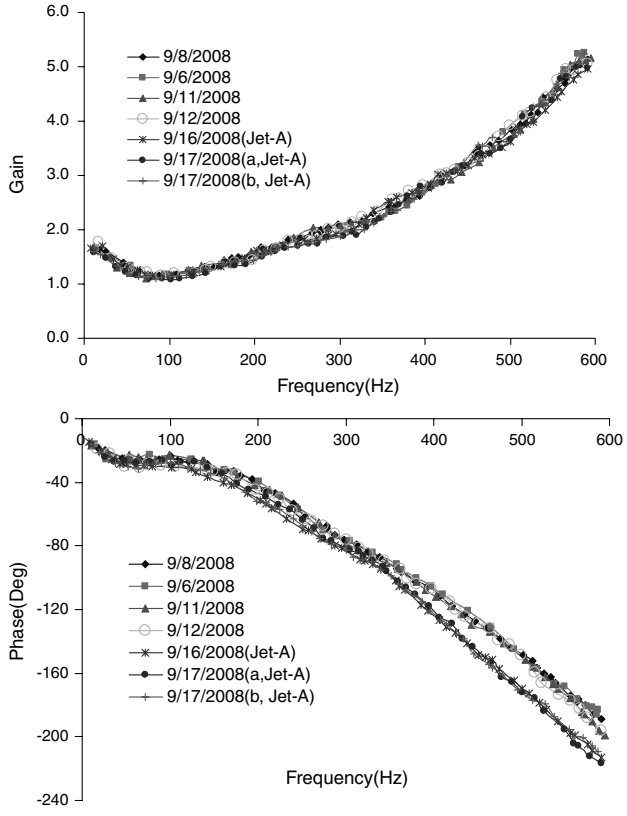

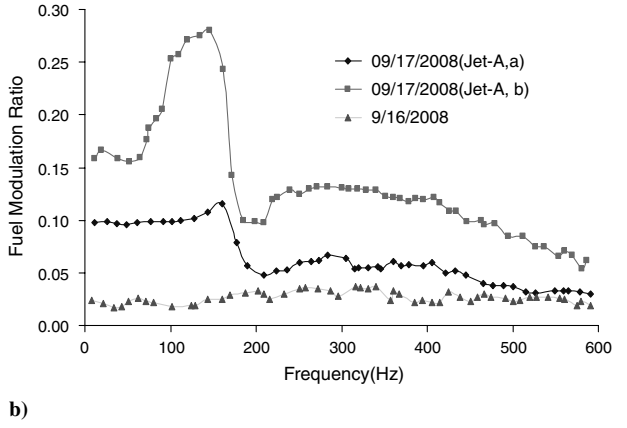

Fig. 8 Measured FTFs and the fuel modulation ratio for experiments conducted on different days: a) FTFs and b) fuel modulation ratio. Mean fuel pressure is 453 kPa, air flow rate is 66.7 g/s, equivalence ratio is 0.34, and preheat temperature is 473 K. The fuel modulation ratio is typically below 2.0%.

transfer, then the evaporation time is estimated as 0.79 ms. Here, the boiling point of 1-decene is taken as 444 K, density as 740 $\mathrm{kg/m^3}$, thermal conductivity of fuel vapor as 0.0532 $\mathrm{W/m \cdot K}$, constant-pressure specific heat as 3059 $\mathrm{J/kg \cdot K}$, and latent heat of vaporization as 286 kJ/kg. Following the procedures in [26], the evaporation constant is determined as $3.25\mathrm{e}-7\ \mathrm{m^2/s}$. From the time-scale analysis, one can see that before the droplets are transported to the major heat release zone, they have fully evaporated. If we assume a laminar flame speed of 0.6 m/s, then the time scale of chemical kinetics can be estimated as [26]

$$\tau_c = \frac{\delta_L}{S_L} \approx \frac{2\alpha}{S_L^2} = 0.79 \text{ ms}$$

Because of the small droplet size and fast fuel/air mixing, combustion characteristics of the current rig is mainly determined by chemical kinetics. This explains why the flame spectra shown in Fig. 2 are very similar to those of lean premixed combustion. The preceding computation gives a rough estimation of time scales for different processes, but the phase lag in the forced flame responses cannot be simply assumed equal to the product of frequency and the sum of the individual time scales. This is because these three processes do not occur sequentially, but rather simultaneously. ICCD images of OH^* chemiluminescence show that the flame is anchored at the forward stagnation point of vortex breakdown and extends along the swirling shear layer.

The flatness in phases below 200 Hz implies the smallness of time delay in the forced flame responses. A pure time-delay unit has a unit gain and an increasing phase lag proportional to frequency. The increasing gain from 240 to 600 Hz implies that the forced flame responses cannot be simply considered as a pure time-delay unit. Rational transfer functions allow both the gain and phases to vary continuously with frequency, which are very convenient for stability analysis and control. A low-order model is developed from the measured FTFs from 240 to 600 Hz:

$$G(z_{-1}) = \frac{\mathrm{CH}^*(z^{-1})}{P_0(z^{-1})} = \frac{-0.4213z^{-2} + 1.604z^{-3} - 1.147z^{-4}}{1 - 1.952z^{-1} + 1.525z^{-2} - 0.5222z^{-3}} \tag{11}$$

As shown in Fig. 9, the low-order model equation (11) closely matches the measured FTFs in both amplitude and phases. The differences are less than 0.5% in amplitude and within 0.5 deg in phases. The FTFs measured on 12 September 2008 are used for model development. The measured FTFs are decomposed into two data segments. One segment is used for model development, and the other is used for validation. The time delay is identified as only one time tap (i.e., 0.2 ms). Given such small time delay, the phase lag shown in Fig. 9 should be associated with a non-time-delay unit, such

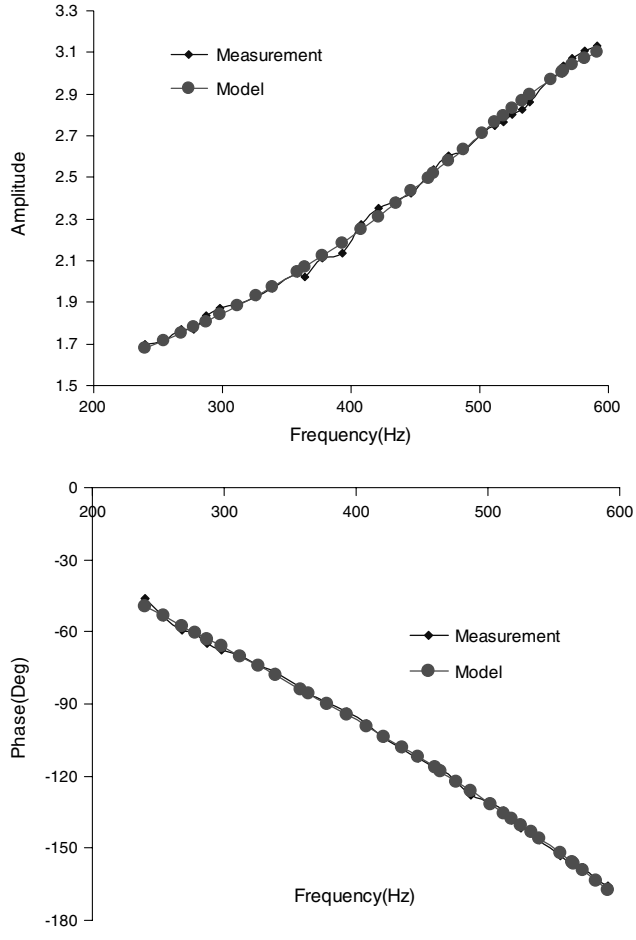

Fig. 9 Measured FTFs vs Bode plots of the low-order models.

as the rational transfer function shown in Eq. (11). Small time delay greatly facilitates combustion analysis and control. In combustion literature [10,12,13], the time delay is typically determined from the slope of the phase curve. If we follow this approach, the time delay will be determined as about 1 ms, which is four times larger than that identified by Eq. (11).

At the preheat temperature of 473 K and the air flow rate of 75.1 g/s (corresponding to a Reynolds number of 97,000), LBO occurs around $\phi = 0.28$. The measured FTF at $\phi = 0.30$ is shown in Fig. 10. Although the equivalence ratio differs by 0.02, insights onto near-LBO combustion dynamics could still be obtained from the measured FTFs at $\phi = 0.30$. The major differences would be the pole locations and the high-frequency gain. At $\phi = 0.28$, because of the exacerbated stability, the poles in the left half phase plane would move closer to the imaginary axis. A low-order model for the FTFs below 200 Hz at $\phi = 0.30$ is derived as follows:

$$G(s) = \frac{67.2618(s + 9793)(s + 1262)}{(s + 326.7)(s^2 + 600.6s + 2.119e6)} \tag{12}$$

This is a third-order, minimum-phase, rational transfer function containing an oscillation mode and zero time delay. As can be seen from Fig. 10, the differences between measurements and modeling are within 1.5% in amplitude and within 1.0 deg in phases.

D. FTFs at Different Air Flow Rates

Shown in Fig. 11 are the FTFs at different air flow rates (44.5, 55.6, and 66.7 g/s, corresponding to a Reynolds number of 68,000, 85,000, and 102,000, respectively) at the same equivalence ratio of 0.36 and the same preheat temperature of 373 K. The computation of the Reynolds number is based on the exit diameter of the air swirler, 3.56 cm, and the average velocity at the swirler exit. The gain of FTFs increases with decreasing air flow rates, whereas the phase lag increases. At a lower air flow rate, the air velocity along the flame front is smaller, which allows the scalar wave (i.e., the equivalence-ratio wave introduced by fuel modulations) to be fully converted into unsteady heat release. At a higher air velocity, the flame is longer, and the flame angle is smaller. Thus, given the same variations in the laminar flame speed caused by equivalence-ratio perturbations, variations in the flame surface area and the heat release rate will be smaller at a higher air flow rate, which results in smaller gain in the FTFs. At lower air flow rates, the convection time or the resident time along the flame front increases, resulting in a larger phase lag. The preceding analysis is rather simple and qualitative. Detailed analysis should model the flame kinematics under equivalence-ratio perturbations and account for the relationship between chemiluminescence and heat release. Low-order modeling of flame kinematics in a turbulent, reacting, swirling shear layer with a large flame angle is extremely challenging because of the complicated physicochemical processes and mathematical tractability. Detailed modeling of flame kinematics is out of the scope of the present study. However, some insights could still be gained from the low-order models summarized in the Introduction. Note that in the presence of equivalence-ratio perturbations, chemiluminescence should not be simply assumed proportional to the instantaneous heat release rate [23]. The relative importance of the reaction heat and the flame surface area in the heat release responses varies with the fuel modulation frequency. For the convenience of readers who are familiar with the normalized flame transfer functions, we plot the gain of $\bar{W}(s)$ in Fig. 12. Note that $\bar{W}(s)$ has the same phase as $W(s)$.

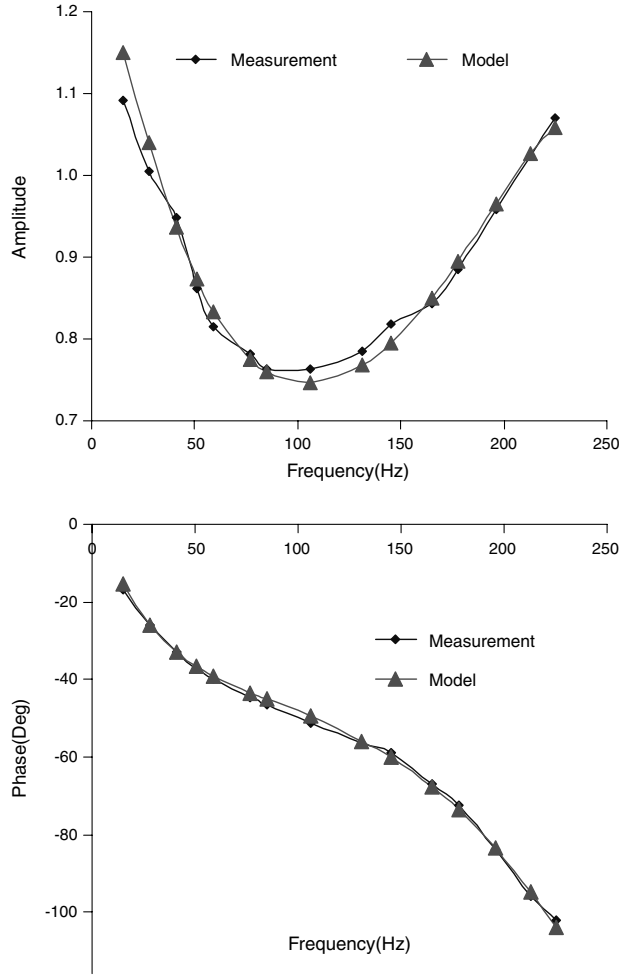

Fig. 10 Low-order models for the measured FTFs at $\phi = 0.30$. Air flow rate is 75.1 g/s, preheat temperature is 473 K, and equivalence ratio is 0.30.

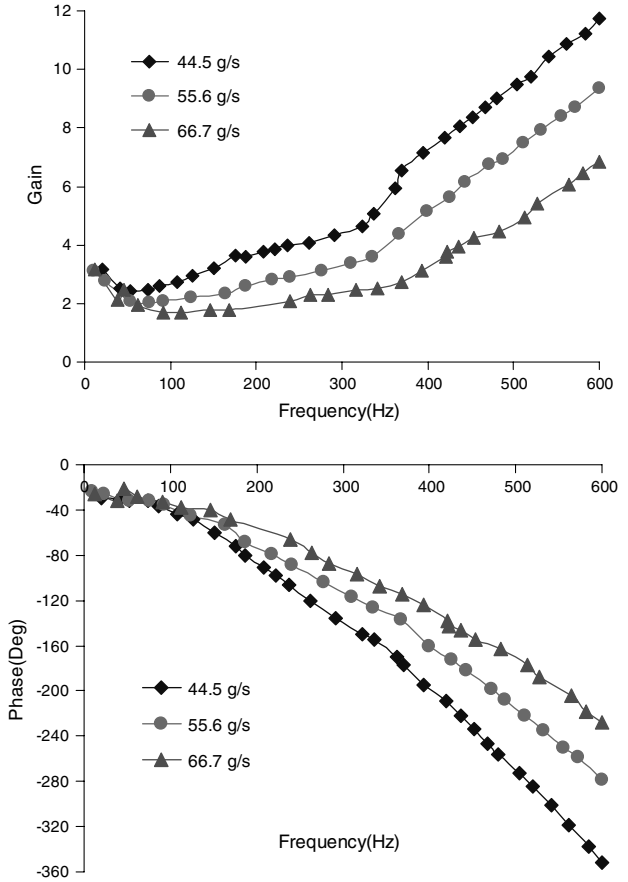

Fig. 11 FTFs at different air flow rates. The fuel modulation ratio is typically below 2.0%, the preheat temperature is 373 K, and the equivalence ratio is 0.36.

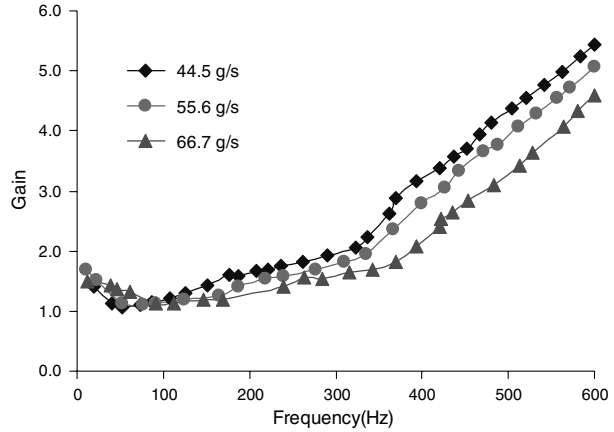

Fig. 12 Gain of the normalized FTFs $\bar{W}(s)$ at different air flow rates. The fuel modulation ratio is typically below 2.0%, the preheat temperature is 373 K, and the equivalence ratio is 0.36.

E. FTFs at Different Equivalence Ratios

Shown in Fig. 13 are the flame transfer functions at different equivalence ratios (0.40, 0.36, and 0.32, respectively), at the same preheat temperature of 373 K and the same air flow rate of 55.6 g/s (corresponding to a Reynolds number of 85,000). Differences in the gain of FTFs between $\phi = 0.40$ and 0.36 are rather small for fuel modulations below 500 Hz. Compared with the FTFs at $\phi = 0.40$ and 0.36, the FTF gain is small at $\phi = 0.32$ and becomes increasingly lower with frequency above 400 Hz. At low equivalence ratios (say, at $\phi = 0.32$), the chemical kinetics and the evaporation rate are rather slow; thus, the flame cannot respond quickly enough to equivalence-ratio perturbations. This is particularly true for high-frequency fuel modulations (say, above 400 Hz). The large phase lag at $\phi = 0.32$ can also be attributed to the slow chemical kinetics and evaporation rates. For the convenience of readers who are familiar with the normalized flame transfer functions, we plot the gain of $\bar{W}(s)$ in Fig. 14. Note that chemiluminescence is a highly nonlinear function of the equivalence ratio. Chemiluminescence intensity at $\phi = 0.32$ is much lower than that at $\phi = 0.40$ and 0.36; thus, the largest gain in $\bar{W}(s)$ is observed at $\phi = 0.32$. However, above 450 Hz, the gain of $\bar{W}(s)$ at $\phi = 0.36$ becomes larger than that at $\phi = 0.32$, which can be attributed to the faster responses in chemical kinetics to equivalence-ratio perturbations at higher flame temperature. It is well known that chemical kinetics has exponential dependence on the flame temperature. From Figs. 13 and 14, one can see that the forced flame responses are nonlinear in terms of the mean equivalence ratio, although they are linear in terms of the fuel modulation amplitude.

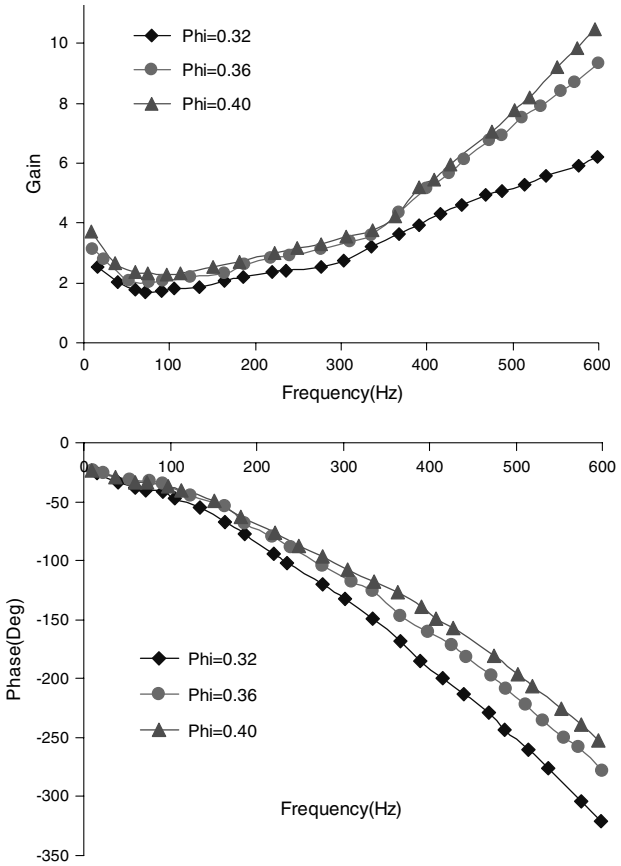

Fig. 13 FTFs at different equivalence ratios. The fuel modulation ratio is typically below 2.0%, the preheat temperature is 373 K, and the air flow rate is 55.6 g/s.

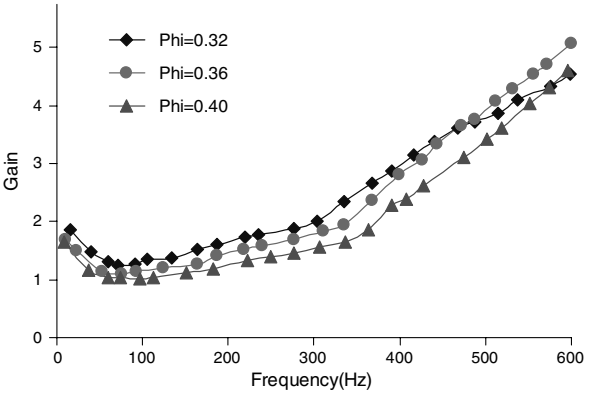

Fig. 14 Gain of the normalized FTFs $\bar{W}(s)$ at different equivalence ratios. The fuel modulation ratio is typically below 2.0%, the preheat temperature is 373 K, and the air flow rate is 55.6 g/s.

F. FTFs at Different Preheat Temperature

Figure 15 shows the FTFs at the preheat temperature of 473, 423, and 373 K, respectively. The air flow rate is 66.7 g/s, and the

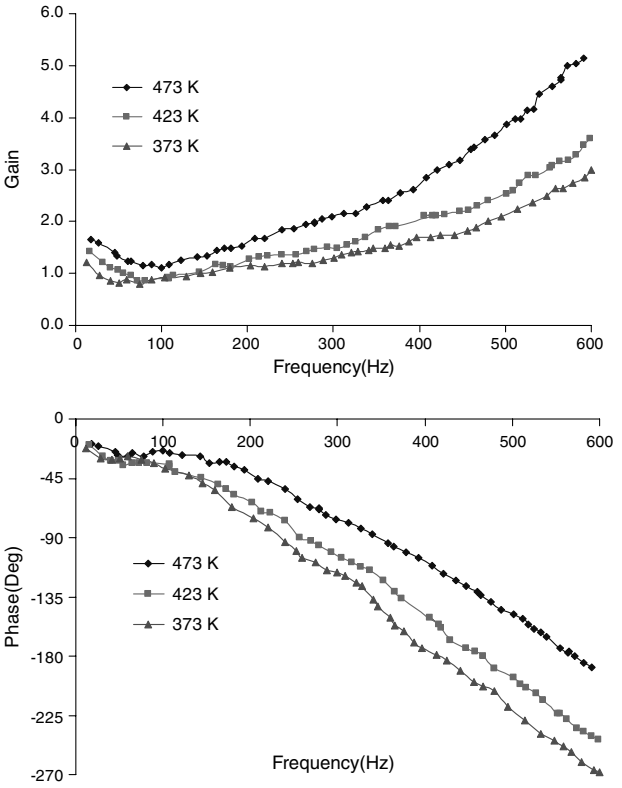

Fig. 15 FTFs at different preheat temperature. The air flow rate is 66.7 g/s, and the equivalence ratio is 0.31.

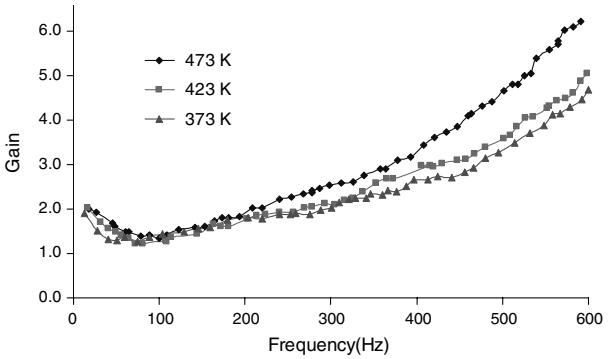

Fig. 16 Gain of the normalized FTFs $\bar{W}(s)$ at different preheat temperature. The air flow rate is 66.7 g/s, and the equivalence ratio is 0.31.

equivalence ratio is 0.31. At the same air flow rate, the air velocity is larger at higher preheat temperature; thus, the residence time decreases, but the time scale of chemical kinetics decreases even further. The flame becomes more responsive to equivalence-ratio perturbations at higher preheat temperature, resulting in larger gain and a smaller phase lag in the FTF. For the convenience of readers who are familiar with the normalized flame transfer functions, we plot the gain of $\bar{W}(s)$ in Fig. 16. Note that $\bar{W}(s)$ has the same phase as $W(s)$. From Figs. 15 and 16, one can see that the FTFs are nonlinear in terms of the preheat temperature, although they are linear in terms of the fuel modulation amplitude.

V. Nonlinear Flame Responses

In this section, we report several nonlinear features in the forced flame responses. The nonlinearity is mainly associated with forcing-induced acoustic feedback around the acoustic resonant frequencies and the interactions between self-excited combustion oscillations and forced flame responses.

A. Effects of Acoustic Damping on Forced Flame Responses

Figure 17 shows the FTFs measured at $\phi = 0.40$ during both stable and unstable combustion. The air flow rate is 44.5 g/s, and the preheat temperature is 373 K. Stable combustion is achieved by inserting three baffle plates downstream of the quartz combustion chamber. Without the baffle plates, the one-wave mode of the combustion chamber is excited around 672 Hz, and the pressure oscillation amplitude is about 15.9 kPa. One can see from Fig. 17 that with different acoustic damping, the differences in the FTFs are quite small except around the acoustic resonant frequencies (i.e., around 340 Hz for the half-wave mode and around 670 Hz for the one-wave mode). With smaller acoustic damping, a much sharper peak appears

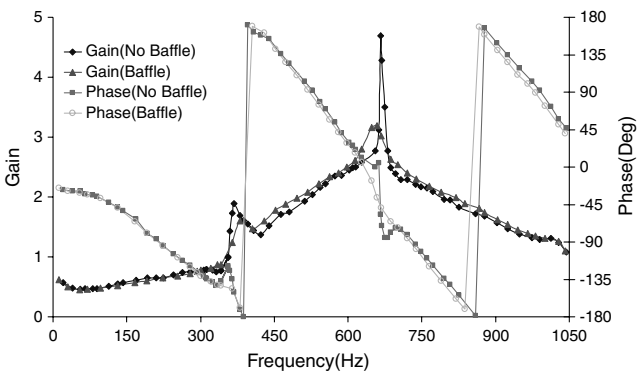

Fig. 17 FTFs for stable combustion vs unstable combustion. The equivalence ratio is 0.40. Stable combustion is achieved by installing three baffle plates downstream of the quartz combustion chamber.

in the FTF gain around 670 Hz, and the phase variations across the resonant frequency are no longer continuous. This can be attributed to the strong forcing-induced acoustic feedback on flame kinematics and chemiluminescence yield. Around the acoustic resonant frequencies, small-amplitude heat release perturbations can generate relatively large acoustic oscillations. Because of the small pressure drop across the air swirler, typically less than 4% in the plenum pressure, small-amplitude pressure oscillations will result in large-amplitude oscillations in the air flow rate into the combustor. The unsteady air flow along the reacting swirling shear layer affects the heat release responses in three aspects. First, it modifies the upstream reactant velocity, which results in variations in the flame surface area and the instantaneous heat release rate; second, it generates equivalence-ratio perturbations because of the differential acoustic impedance between the fuel and air lines, which results in variations in the laminar flame speed and the flame kinematics; and third, acoustic oscillations themselves affect the heat release dynamics via variations in the reactant density and chemical kinetics.

B. Extinction and Entrainment of Self-Excited Combustion Oscillations by Fuel Modulations

Interactions between self-excited combustion oscillations and external forcing, which has been widely studied in structural vibrations [27], are seldom reported in combustion community. The only relevant study seems to be performed by Bellows et al. [28] on a 10 kW, premixed, natural-gas-fueled, atmospheric combustor forced by two speakers. In the present study, we apply high-frequency fuel modulations to a liquid-fueled, swirl-stabilized, LDI combustor shown in Fig. 1.

At the air flow rate of 44.5 g/s, the equivalence ratio of 0.40, and the preheat temperature of 373 K, self-excited combustion instability occurs around 672 Hz (one-wave mode). The baseline oscillation amplitude is 15.9 kPa for the combustor pressure and is 0.8 a.u. (atomic units) for CH^* chemiluminescence. The mean chemiluminescence is 3.40 a.u. At the approach of the acoustic resonant frequency from 640 Hz, with the same amount of fuel modulations,

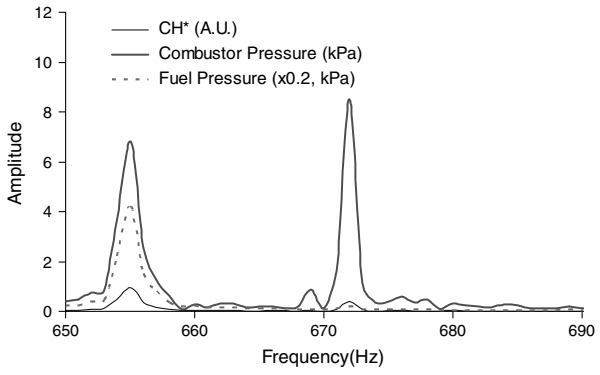

a)

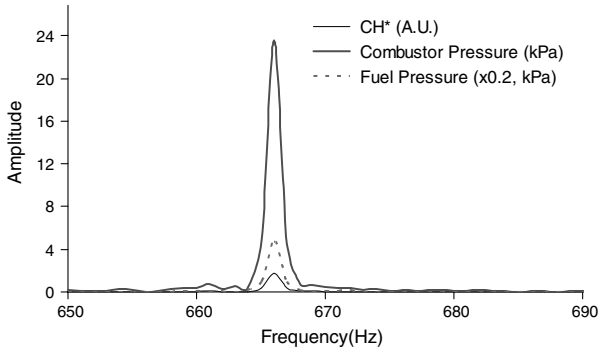

b)

Fig. 18 Spectra of combustor pressure and chemiluminescence with fuel modulations around the acoustic resonant frequencies: a) fuel modulations at 655 Hz and b) fuel modulations at 666 Hz.

the amplitude of self-excited combustion oscillations consistently decreases, and it completely disappears with fuel modulations at 666 Hz. Fuel modulations below 640 Hz have few effects on self-excited combustion instability. Figure 18 shows the spectra of combustor pressure and chemiluminescence with fuel modulations at 655 and 666 Hz, respectively. The oscillation amplitude of fuel pressure is the same: 5.0% of the mean fuel pressure. At the approach of the acoustic resonant frequency, although self-excited combustion oscillations are diminished, forcing-induced acoustic oscillations are vigorously intensified. In particular, with fuel modulations at 666 Hz, the amplitude of forcing-induced pressure oscillations is about 50% stronger than the baseline oscillations. Attenuation of self-excited combustion oscillations can also be achieved by increasing the amplitude of fuel modulations nearby the limit-cycle oscillation frequency. Limited by the paper length, detailed results are not shown here. Forced flame responses around the acoustic resonant frequencies shed valuable insights onto the underlying physics of combustion instability, but they are not a practical approach for combustion instability attenuation. Interestingly, open-loop fuel modulations at very low frequencies (say, at 11 Hz) are very effective in attenuating self-excited combustion oscillations. As shown in Fig. 19, self-excited combustion oscillations can be effectively attenuated by increasing fuel modulations at 11 Hz. Here, the fuel modulation amplitude is normalized by the mean fuel pressure of 276 kPa. Because the acoustic resonant frequencies are much higher than 11 Hz, large-amplitude fuel modulations up to 30% of the mean fuel pressure can only generate small-amplitude acoustic oscillations of less than 15% of the limit-cycle oscillation amplitude. Richards et al. [29] have also observed the effectiveness of low-frequency fuel modulations on combustion instability suppression and proposed that the forcing period is commensurate with the growth and decay rates of self-excited combustion oscillations.

VI. Applications of FTFs

The FTFs can be directly used for combustion control design. Active control of both phenomena can be achieved using small-amplitude fuel modulations, employing the same control hardware and fuel actuators. There is also a high possibility that one adaptive control algorithm can control both phenomena, because small-amplitude fuel modulations can affect both combustion instability and LBO. However, several major differences exist between combustion instability control and LBO extension. First, combustion instability is linearly unstable, but near-LBO combustion dynamics is linearly stable. Stable combustion cannot be maintained at all if the equivalence ratio drops below the flammability limits. Second, because combustion instability is linearly unstable, the fuel actuator should keep working to prevent acoustic pressure from regaining energy, even after the initial strong pressure pulsations have been suppressed. However, for LBO control, no further fuel actuations are required after the initial deviations from the equilibrium points have been diminished. Third, combustion instability is temporally and spatially coherent and occurs around the acoustic resonant frequency. But near-LBO, combustion dynamics are typically much less coherent and usually occur below 200 Hz. This implies that for LBO control, the actuator bandwidth and time delay associated with fuel convection, evaporation, and chemical kinetics may not be major technical challenges.

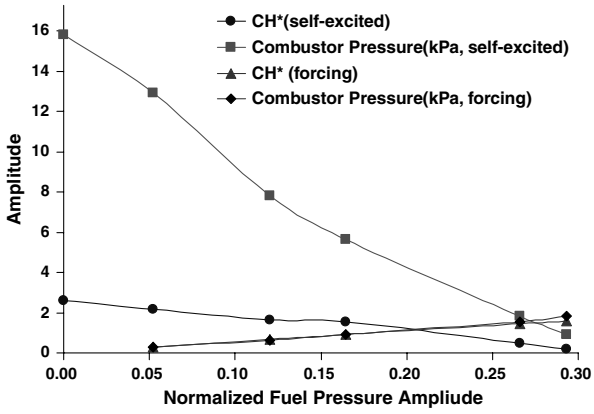

Fig. 19 Attenuation of self-excited combustion oscillations around 672 Hz with fuel modulations at 11 Hz.

A. Combustion Instability Control

If no variations occur in the flame structure, which is usually true during the initial stage of combustion instability and weak oscillations, the derived FTFs can be directly used for control design. The controller can be simply designed to provide an external heat release perturbation to counteract the self-excited heat release oscillations. The FTFs developed in this paper are based on the heat release responses instead of pressure responses. The advantage of using chemiluminescence as the sensor signal is that the measured FTFs can be conceived as an intrinsic property of the burner alone if forcing-induced pressure oscillations are small. This can be achieved by using a short combustion chamber to increase the fundamental resonant frequency and by installing baffle plates and resonators to enhance acoustic damping. In this way, when the same type of burner is used in different combustors or engines, even if the resonant frequencies are different, the same control algorithm can be used. Pressure sensing has been widely used for combustion instability control. Around the acoustic resonant frequencies, the pressure signal typically has a higher signal-to-noise ratio than chemiluminescence. This is because a combustion system can be conceived as a kind of bandpass filter that has large gain around the acoustic resonant frequencies. If pressure is used as the sensing signal, a low-order model accounting for the relationship between the heat release rate and pressure should be developed before the measured FTFs can be used for feedback control design. As shown in [23], the relationship between the instantaneous heat release rate and chemiluminescence is rather complicated.

B. LBO Control

With decreasing equivalence ratios toward the lean flammability limits, a combustor's resistance to external disturbances or deviations from the equilibrium point is considerably weakened. If the initial small deviations from the equilibrium points can be quickly damped out using a feedback controller, the state trajectory will have no opportunity to grow and cross the catastrophic boundary. Muruganandam et al. [30] have demonstrated LBO extension by increasing the amount of pilot fuel, based on the detection of LBO precursor events. Here, we propose that small-amplitude fuel modulations based on modern feedback control strategies be used to enhance near-LBO combustion stability. This control approach has fast responses, and the spatial distribution of fuel is not modified. In addition, the low-frequency near-LBO chemiluminescence oscillations are directly used for feedback control design; thus, the algorithms for detecting incipient LBO are not required. Stability enhancement of near-LBO combustion using a simple linear quadratic Gaussian feedback controller has been numerically demonstrated in [3]. Because an aeroengine has to operate within a large range of working conditions, adaptive robust controllers, which have superior robust stability and control performance, are promising. The measured near-LBO flame transfer functions have no unstable zeros, no unstable poles, and even negligibly small time delay; thus, an adaptive robust controller can be worked out quite straightforwardly. In addition to liquid-fueled LDI combustion, the developed LBO control strategy can also be used for gas-fueled combustion, such as syngas combustion. Because of large variations in feedstocks, the ratio of H_2/CO in syngas can change from 0.33 to 40, and the concentration of water vapor can vary from 0 to 40% [31]. This represents significant challenges to stable combustion, at very lean conditions in particular. Near-LBO combustion dynamics may exhibit persistent low-frequency oscillations [30,32] or undergo partial or global quenching without showing much oscillatory behavior. Both situations can be handled by the feedback controller.

VII. Conclusions

1) A motor-driven rotary fuel valve specially designed for fuel modulations up to 1 kHz is used for forced flame response measurements. The fuel modulation ratio is controlled by adjusting fuel split between the rotary valve and a bypass passage. The flame spectra of the liquid-fueled, swirl-stabilized, LDI combustor are very similar to those of lean, premixed, gaseous combustion. This can be attributed to the small droplet size and fast fuel/air mixing.

2) A method for determination of the instantaneous fuel flow rate out of a liquid fuel nozzle is developed, which is based on the acoustic wave theory and pressure measurements upstream of the fuel nozzle. Differences between pressure measurements and prediction are within 6% in amplitude and 6 deg in phases.

3) Good signal-to-noise ratios above 20 dB can be achieved with a fuel modulation ratio above 0.5%. Repeatability and linearity in the measured FTFs are demonstrated. The derived FTFs are not sensitive to variations in the fuel modulation amplitude, implying that the derived FTFs are linear and that the induced heat release rate oscillations are mainly caused by variations in the instantaneous fuel flow rate instead of in the droplet size and distribution. Low-order models in the form of a rational transfer function are developed from the measured gain and phases, which can be conveniently used for stability analysis and control design.

4) Effects of the air flow rate, the equivalence ratio, and the preheat temperature on the FTFs are examined. The phase lag decreases with the air flow rate, the equivalence ratio, and the preheat temperature, which can be attributed to the smaller time scales in convection and chemical kinetics. The gain increases with the equivalence ratio and the preheat temperature and decreases with the air flow rate. The measured flame transfer functions are linear in terms of the fuel modulation amplitude, but nonlinear in terms of the air flow rate, the preheat temperature, and the equivalence ratio. Normalized flame transfer functions are also provided.

5) Nonlinearity in the forced flame responses, including the effects of acoustic damping on the FTFs around the acoustic resonant frequencies and interactions between self-excited combustion oscillations and fuel modulations, are experimentally observed. Open-loop fuel modulations nearby the acoustic resonant frequencies are not a practical strategy for combustion instability attenuation, but low-frequency fuel modulations may show some promise.

6) Applications of the FTFs to combustion control, including both combustion instability and lean blowout, are discussed. If no variations occur in the flame structure, which is usually true during the initial stage of combustion instability and weak oscillations, the derived FTFs can be directly used for control design. The proposed control strategy can also be used for gas-fueled combustion.

Acknowledgments

Support from NASA John H. Glenn Research Center at Lewis Field under grant NNX07C98A, "Active Combustion Control for Low-Emission Combustors," is gratefully acknowledged (Clarence Chang is the project manager). This project is also supported by U.S. Air Force under grant FA9550-07-1-0451, "Advanced Thermally Stable Coal-Based Jet Fuels."

References

[1] Lieuwen, T. C., and Yang, V. (eds.), *Combustion Instabilities in Gas Turbine Engines: Operational Experience, Fundamental Mechanisms, and Modeling*, Progress in Astronautics and Aeronautics, Vol. 210, AIAA, Reston, VA, 2005, p. 657.

[2] Yi, T., and Gutmark, E. J., "Stability and Control of Lean Blowout in Chemical Kinetics—Controlled Combustion Systems," *Combustion Science and Technology*, Vol. 181, No. 2, 2009, pp. 226–244. doi:10.1080/00102200802424559

[3] Yu, K. H., and Wilson, K. J., "Scale-Up Experiments on Liquid-Fueled Active Combustion control," *Journal of Propulsion and Power*, Vol. 18, No. 1, 2002, pp. 53–60. doi:10.2514/2.5897

[4] Duvvur, A., Chiang, C. H., and Sirignano, W. A., "Oscillatory Fuel Droplet Vaporization: Driving Mechanism for Combustion Instability," *Journal of Propulsion and Power*, Vol. 12, No. 2, 1996, pp. 358–365. doi:10.2514/3.24036

[5] Marble, F. E., and Candel, S. M., "An Analytical Study of the Nonsteady Behavior of Large Combustors," *Proceedings of the Combustion Institute*, Vol. 17, 1978, pp. 761–769.

[6] You, D., Huang, Y., and Yang, V., "A Generalized Model of Acoustic Response of Turbulent Premixed Flame and Its Application to Gas Turbine Combustion Instability Analysis," *Combustion Science and Technology*, Vol. 177, Nos. 5–6, 2005, pp. 1109–1150. doi:10.1080/00102200590927012

[7] Preetham, S. H., and Lieuwen, T. C., "Response of Turbulent Premixed Flames to Harmonic Acoustic Forcing," *Proceedings of the Combustion Institute*, Vol. 31, No. 1, 2007, pp. 1427–1434. doi:10.1016/j.proci.2006.07.198

[8] Cho, J. H., and Lieuwen, T. C., "Laminar Premixed Flame Response to Equivalence Ratio Oscillations," *Combustion and Flame*, Vol. 140, Nos. 1–2, 2005, pp. 116–129. doi:10.1016/j.combustflame.2004.10.008

[9] Fleifil, M., Annaswamy, A. M., Ghohiem, Z. A., and Ghoniem, A. F., "Response of a Laminar Premixed Flame to Flow Oscillations: A Kinematic Model and Thermoacoustic Instability Results," *Combustion and Flame*, Vol. 106, No. 4, 1996, pp. 487–510. doi:10.1016/0010-2180(96)00049-1

[10] Lieuwen, T. C., "Nonlinear Kinematic Response of Premixed Flames to Harmonic Velocity Disturbances," *Proceedings of the Combustion Institute*, Vol. 30, No. 2, 2005, pp. 1725–1732. doi:10.1016/j.proci.2004.07.020

[11] Schuller, T., Durox, D., and Candel, S., "A Unified Model for the Prediction of Laminar Flame Transfer Functions: Comparisons between Conical and *V*-Flame Dynamics," *Combustion and Flame*, Vol. 134, Nos. 1–2, 2003, pp. 21–34. doi:10.1016/S0010-2180(03)00042-7

[12] Kim, D., Lee, J. G., Quay, B. D., and Santavicca, D., Kim, K., and Srinivasan, S., "Effect of Flame Structure on the Flame Transfer Function in a Premixed Gas Turbine Combustor," ASME Turbo Expo 2008, American Society of Mechanical Engineers Paper GT2008-51014, Berlin, 2008.

[13] Kim, K. T., Lee, J. G., Lee, H. J., Quay, B. D., and Santavicca, D. A., "Characterization of Forced Flame Response of Swirl-Stabilized Turbulent Premixed Flames," ASME Turbo Expo 2009, Orlando, FL, American Society of Mechanical Engineers Paper GT2009-60031, 2009.

[14] Balachandran, R., Ayoola, B. O., Kaminski, C. F., Dowlinga, A. P., and Mastorakos, E., "Experimental Investigation of the Nonlinear Response of Turbulent Premixed Flames to Imposed Inlet Velocity Oscillations," *Combustion and Flame*, Vol. 143, Nos. 1–2, 2005, pp. 37–55. doi:10.1016/j.combustflame.2005.04.009

[15] Dowling, A. P., "Nonlinear Self-Excited Oscillations of a Ducted Flame," *Journal of Fluid Mechanics*, Vol. 346, 1997, pp. 271–290. doi:10.1017/S0022112097006484

[16] Culick, F. E. C., "Combustion Instabilities in Liquid-Fueled Propulsion Systems—An Overview," AGARD/NATO CP-450, Neuilly-sur-Seine, France, 1989.

[17] Wee, D., Yi, T., Annaswamy, A. M., and Ghoniem, A. F., "Self-Sustained Oscillations and Vortex Shedding in Backward-Facing Step Flows: Simulation and Linear Instability Analysis," *Physics of Fluids*, Vol. 16, No. 9, 2004, pp. 3361–3373. doi:10.1063/1.1773091

[18] Syred, N., and Beer, J. M., "Combustion in Swirling Flows: A Review," *Combustion and Flame*, Vol. 23, No. 2, 1974, pp. 143–201. doi:10.1016/0010-2180(74)90057-1

[19] Lilly, D. G., "Swirling Flow in Combustion: a Review," *AIAA Journal*, Vol. 15, No. 8, 1977, pp. 1063–1078. doi:10.2514/3.60756

[20] Yi, T., and Santavicca, D. A., "Combustion Instability in a Turbulent Liquid-Fueled Swirl-Stabilized LDI Combustor," 45th AIAA/ASME/SAE/ASEE Joint Propulsion Conference and Exhibit, AIAA Paper 2009-5014, Denver, CO, 2009.

[21] Anderson, T., and Morford, S., "Dynamic Flame Structure in a Low NO_x Premixed Combustor," ASME Turbo Expo 1998, American Society of Mechanical Engineers Paper GT98-568, Stockholm, June 1998.

[22] Eckstein, J., Freitag, E., Hirsch, C., Sattelmayer, T., Von Der Bank, R., and Schilling, T., "Forced Low-Frequency Spray Characteristics of a Generic Airblast Swirl Diffusion Burner," *Journal of Engineering for Gas Turbines and Power*, Vol. 127, No. 2, 2005, pp. 301–306. doi:10.1115/1.1789515

[23] Yi, T., and Santavicca, D. A., "Flame Spectra of a Liquid-Fueled Swirl-Stabilized LDI Combustor," *Journal of Propulsion and Power*, Vol. 25,

No. 5, 2009, pp. 1058–1067.
doi:10.2514/1.43003

[24] Yi, T., and Santavicca, D. A., "Determination of the Instantaneous Fuel Flow Rate Out of a Fuel Injector," *Journal of Engineering for Gas Turbines and Power*, Vol. 132, No. 1, 2009.

[25] *Coordinating Research Council, Handbook of Aviation Fuel Properties*, 3rd ed., SAE International, Warrendale, PA, 2004.

[26] Turns, S. R., *An Introduction to Combustion: Concepts and Applications*, 2nd ed., McGraw–Hill, New York, 2000, pp. 362–378, 461.

[27] Nayfeh, A. H., *Nonlinear Oscillations*, Wiley-Interscience, New York, May 1979.

[28] Bellows, B. D., Hreiz, A., and Lieuwen, T., "Nonlinear Interactions Between Forced and Self-Excited Acoustic Oscillations in Premixed Combustor," *Journal of Propulsion and Power*, Vol. 24, No. 3, 2008, pp. 628–631.
doi:10.2514/1.33228

[29] Richards, G. A., Thornton, J. D., Robey, E. H., and Arellano, L., "Open-Loop Active Control of Combustion Dynamics on a Gas Turbine Engine," *Journal of Engineering for Gas Turbines and Power*, Vol. 129, 2007, pp. 38–48.
doi:10.1115/1.2204978

[30] Muruganandam, T. M., Nair, S., Scarborough, D., Neumeier, Y., Jagoda, J., Lieuwen, T., Seitzman, J., and Zinn, B., "Active Control of Lean Blowout for Turbine Engine Combustors," *Journal of Propulsion and Power*, Vol. 21, No. 5, 2005, pp. 807–812.
doi:10.2514/1.7254

[31] Moliere, M., "Benefiting from the Wide Fuel Capability of Gas Turbines: a Review of Application Opportunities," ASME Turbo Expo 2002, American Society of Mechanical Engineers Paper GT2002-30017, Amsterdam, June 2002.

[32] Yi, T., and Gutmark, E. J., "Real-Time Prediction of Incipient Lean Blowout in Gas Turbine Combustors," *AIAA Journal*, Vol. 45, No. 7, 2007, pp. 1734–1739.
doi:10.2514/1.25847

A. Gupta
Associate Editor